

# Multidimensional *en-Face* OCT imaging of the retina <sup>◇</sup>

Richard B. Rosen,<sup>1,5</sup> Mark Hathaway,<sup>2,4</sup> John Rogers,<sup>2</sup> Justin Pedro,<sup>2</sup> Patricia Garcia,<sup>1</sup>  
Philippe Laissue,<sup>3</sup> George M. Dobre,<sup>4</sup> Adrian Gh. Podoleanu<sup>4,5,\*</sup>

<sup>1</sup>Advanced Retinal Imaging Center, New York Eye and Ear Infirmary, New York, New York, USA,  
and New York Medical College, Valhalla, New York, USA

<sup>2</sup>Ophthalmic Technologies Inc., Toronto, Canada

<sup>3</sup>Neurosciences and Medical Image Computing Group, Department of Biosciences,  
University of Kent, Canterbury, Kent CT2 7NJ, UK

<sup>4</sup>Applied Optics Group, University of Kent, Canterbury, CT2 7NH, UK

<sup>5</sup>Contributed equally to the work and therefore should be considered equivalent authors

\*Corresponding author: [A.G.H.Podoleanu@ukc.ac.uk](mailto:A.G.H.Podoleanu@ukc.ac.uk)

**Abstract:** Fast T-scanning (transverse scanning, *en-face*) was used to build B-scan or C-scan optical coherence tomography (OCT) images of the retina. Several unique signature patterns of *en-face* (coronal) are reviewed in conjunction with associated confocal images of the fundus and B-scan OCT images. Benefits in combining T-scan OCT with confocal imaging to generate pairs of OCT and confocal images similar to those generated by scanning laser ophthalmoscopy (SLO) are discussed in comparison with the spectral OCT systems. The multichannel potential of the OCT/SLO system is demonstrated with the addition of a third hardware channel which acquires and generates indocyanine green (ICG) fluorescence images. The OCT, confocal SLO and ICG fluorescence images are simultaneously presented in a two or a three screen format. A fourth channel which displays a live mix of frames of the ICG sequence superimposed on the corresponding coronal OCT slices for immediate multidimensional comparison, is also included. OSA ISP software is employed to illustrate the synergy between the simultaneously provided perspectives. This synergy promotes interpretation of information by enhancing diagnostic comparisons and facilitates internal correction of movement artifacts within C-scan and B-scan OCT images using information provided by the SLO channel.

©2009 Optical Society of America

**OCIS codes:** (170.4470) Ophthalmology; (170.4500) Optical coherence tomography;  
(170.3890) Medical optics instrumentation.

<sup>◇</sup>Datasets associated with this article are available at <http://hdl.handle.net/10376/1199>.

---

## References and links

1. R. Leitgeb, C. K. Hitzenberger, and A. F. Fercher, "Performance of Fourier domain vs. time domain optical coherence tomography," *Opt. Express* **11**, 889–894 (2003).
2. J. F. de Boer, B. Cense, B. H. Park, M. C. Pierce, G. J. Tearney, and B. E. Bouma, "Improved signal-to-noise ratio in spectral-domain compared with time-domain optical coherence tomography," *Opt. Lett.* **28**, 2067–2069 (2003).
3. A. Gh. Podoleanu, G. M. Dobre, and D. A. Jackson, "*En-face* coherence imaging using galvanometer scanner modulation," *Opt. Lett.* **23**, 147–149 (1998).
4. A. Gh. Podoleanu, M. Seeger, G. M. Dobre, D. J. Webb, D. A. Jackson, and F. Fitzke, "Transversal and longitudinal images from the retina of the living eye using low coherence reflectometry," *J. Biomed. Opt.* **3**, 12–20 (1998).
5. C. C. Rosa, J. Rogers, J. Pedro, R. Rosen, and A. Podoleanu, "Multi-scan time domain OCT for retina imaging," *Appl. Opt.* **46**, 1795–1807 (2007).

6. A. Gh. Podoleanu and D. A. Jackson, "Combined optical coherence tomograph and scanning laser ophthalmoscope," *Electron. Lett.* **34**, 1088–1090 (1998).
7. M. Pircher, E. Gotzinger, and C. K. Hitzenberger, "Dynamic focus in optical coherence tomography for retinal imaging," *J. Biomed Opt.* **11**, 054013 (2006).
8. M. Pircher, B. Baumann, E. Göttinger, and C. K. Hitzenberger, "Retinal cone mosaic imaged with transversal scanning OCT," *Opt. Lett.* **31**, 1821–1823 (2006).
9. S. Tuohy, A. Bradu, A. Gh. Podoleanu, and N. Chateau, "Correcting ocular aberrations with a high stroke deformable mirror," *Proc.SPIE* **6627** 66271L (2007).
10. D. Merino, Ch. Dainty, A. Bradu, and A.Gh. Podoleanu, "Adaptive optics enhanced simultaneous *en-face* optical coherence tomography and scanning laser ophthalmoscopy," *Opt. Express* **14**, 3345–3353 (2006).
11. M. Pircher, R. J. Zawadzki, J. W. Evans, J. S. Werner, and C. K. Hitzenberger, "Simultaneous imaging of human cone mosaic with adaptive optics enhanced scanning laser ophthalmoscopy and high-speed transversal scanning optical coherence tomography," *Opt. Lett.* **33**, 22–24 (2008).
12. A. Gh. Podoleanu and R. B. Rosen, "Combinations of techniques in imaging the retina with high resolution," *Prog. Retin. Eye Res.* **27**, 464–499 (2008).
13. C. K. Hitzenberger, P. Trost, P. Lo, and Q. Zhou, "Three-dimensional imaging of the human retina by high-speed optical coherence tomography," *Opt. Express* **11**, 2753–2761 (2003).
14. R. Huber, D. C. Adler, V. G. Srinivasan, and J. G. Fujimoto, "Fourier domain mode locking at 1050 nm for ultra-high-speed optical coherence tomography of the human retina at 236,000 axial scans per second," *Opt. Letters* **32**, 2049–2051 (2007).
15. A. Gh. Podoleanu, G. M. Dobre, R. G. Cucu, R. B. Rosen, P. Garcia, J. Nieto, D. Will, R. Gentile, T. Muldoon, J. Walsh, L. A. Yannuzzi, Y. Fisher, D. Orlock, R. Weitz, J. A. Rogers, S. Dunne, and A. Boxer, "Combined multiplanar optical coherence tomography and confocal scanning ophthalmoscopy," *J. Biomed. Opt.* **9**, 86–93 (2004).
16. A. Gh. Podoleanu and D. A. Jackson, "Noise analysis of a combined optical coherence tomograph and a confocal scanning ophthalmoscope," *Appl. Opt.* **38**, 2116–2127 (1999).
17. B. R. Masters, "Three-dimensional confocal microscopy of the human optic nerve in vivo," *Opt. Express* **3**, 356–359 (1998).
18. A. Gh. Podoleanu, I. Charalambous, L. Plesea, A. Dogariu, and R. B. Rosen, "Correction of distortions in OCT imaging of the eye," *Phys. Med. Biol.* **49**, 1277–1294 (2004).
19. R. G. Cucu, A.Gh. Podoleanu, A. Rogers, J. Pedro, and R. B. Rosen, "Combined confocal scanning ophthalmoscopy/en face T-scan based ultrahigh resolution OCT of the human retina in vivo," *Opt. Lett.* **31**, 1684–1687 (2006).
20. A. Gh. Podoleanu, G. M. Dobre, R. Cernat, J. A. Rogers, J. Pedro, R. B. Rosen, and P. Garcia, "Investigations of the eye fundus using a simultaneous optical coherence tomography/indocyanine green fluorescence imaging system," *J. Biomed. Opt.* **12**, 014019 (2007).
21. M. Wojtkowski, V. Srinivasan, J. G. Fujimoto, T. Ko, J. S. Schuman, A. Kowalczyk, and J. S. Duker, "Three dimensional retinal imaging with high-speed ultrahigh-resolution optical coherence tomography," *Ophthalmology* **112**, 1734–1746 (2005).
22. H. Lim, M. Mujat, C. Kerbage, E. C. Lee, Y. Chen, T. C. Chen, and J. F. de Boer, "High-speed imaging of human retina in vivo with swept-source optical coherence tomography," *Opt. Express* **14**, 12902–12908 (2006).
23. M. E. J. Van Velthoven, F. D. Verbraak, L. A. Yannuzzi, R. B. Rosen, A. Gh. Podoleanu, and M. D. De Smet, "Imaging the retina by *en-face* optical coherence tomography," *Retina* **26**, 129–136 (2006).
24. Y. Hong, S. Makita, M. Yamanari, M. Miura, S. Kim, T. Yatagai, and Y. Yasuno, "Three-dimensional visualization of choroidal vessels by using standard and ultra-high resolution scattering optical coherence angiography," *Opt. Express* **15**, 7538–7550 (2007).
25. S. L. Jiao, C. Y. Wu, R. W. Knighton, G. Gregori, and C. A. Puliafito, "Registration of high-density cross sectional images to the fundus image in spectral-domain ophthalmic optical coherence tomography," *Opt. Express* **14**, 3368–3376 (2006).
26. Y. Yasuno, Y. J. Hong, M. Makita, M. Yamanari, M. Akiba, M. Miura, and T. Yatagai, "In vivo high-contrast imaging of deep posterior eye by 1- $\mu$ m swept source optical coherence tomography and scattering optical coherence angiography," *Opt. Express* **15**, 6121–6139 (2007).
27. M. Pircher, B. Baumann, E. Goetzinger, H. Sattmann, and C. K. Hitzenberger, "Simultaneous SLO/OCT imaging of the human retina with axial eye motion correction," *Opt. Express* **15**, 16922–16932 (2007).
28. P. Thévenaz, U.E. Ruttimann, and M. Unser, "A pyramid approach to subpixel registration based on intensity," *IEEE Trans. Image Process.* **7**, 27–41 (1998).
29. MATLAB, <http://www.mathworks.com/products/matlab>.

## 1. Introduction

High resolution imaging and tomographic assessments in the ocular fundus have been greatly enhanced with the introduction of the spectral-domain optical coherence tomography (SD-

OCT). In SD-OCT, cross section images (B-scans) are generated from A-scans (depth reflectivity profiles). Due to its enhanced signal to noise ratio [1,2], faster acquisition rates are achievable compared to classic time domain OCT (TD-OCT).

SD-OCT methods, while fast and increasingly popular across a wider community of OCT developers and ophthalmologists, nevertheless suffer from some significant limitations: (i) artifactual mirror images, (ii) limited depth of scan capability and decay of sensitivity with depth, (iii) incompatibility with dynamic focus and (iv) limited compatibility with a live fundus image. In comparison, TD-OCT has a constant sensitivity with depth, is compatible with dynamic focus and is not affected by artifactual mirror images.

One version of TD-OCT, *en-Face (eF)* OCT, creates images by employing transversal priority scanning (T-scans) [3]. In the *eF*-OCT, images are generated from many T-scans. These are transversal profiles of reflectivity generated by scanning the optical beam transversally, along different trajectories (raster, helicoidal, etc).

*eF*-OCT offers certain advantages. First, T-scans can be used to generate B-scans as well as coronal plane oriented scans (C-scans) [4]. This allows *eF*-OCT technology to perform quick alternating imaging sessions in orthogonal planes by instantly switched scanning regimes [5].

Second, the technology is compatible with live and simultaneous generation of a conventional fundus image (coronal-plane oriented) [6].

Third, the *eF*-OCT is ideal for dynamic focus. While in general, TD-OCT is compatible with dynamic focus, it is hard to implement dynamic focus in an A-scan based TD-OCT system because the focus adjustment needs to be synchronized with the A-scanning, which is fast and determined by the line scanning rate. In contrast, with *eF*-OCT, the demand for the focus adjustment is relaxed, as the focus adjustment needs to be performed at the frame rate, which is of much lower frequency rate. The power of this technology has been demonstrated using a bulk interferometer system equipped with dynamic focus, to image the cone mosaic simultaneously in the SLO and OCT channels without adaptive optics elements (AO) [7, 8].

The importance of dynamic focus is expected to become more important in the near future as progress in AO assisted OCT accelerates. When the AO loop manages to achieve ideal correction, A-scan based OCT methods would be limited to collecting signals from a much reduced depth range. Therefore, *eF*-OCT might turn out to be a better choice for combination with AO, than any other OCT methods [9, 10, 11].

The recent attention given to SD-OCT is justified by the increase in the amount of megavoxels acquired per second [12]. TD-OCT methods (either A-scan based or T-scan based) cannot currently compete with SD-OCT in this respect. This makes the TD-OCT methods, including the *eF*-OCT less attractive in creating volumes of the tissue, due to the long time required to collect data from a significant volume (tens of seconds when using galvo-scanners and several seconds when using resonant scanners [13] in comparison with a few seconds or less than 1 s in SD-OCT, as proven recently using the swept source-OCT method [14]).

The ability to image live thin sections of the retina alongside a corresponding live fundus image, provides a uniquely exciting capability for the ophthalmologist. In the last 5 years, the SD-OCT developers have investigated several approaches to generation of fundus images from SD-OCT data. These have all attempted to provide accurate localization and meaningful contextual orientation of OCT cross-sections to fundus landmarks. This facility is inherent in T-scan based TD-OCT.

This paper presents an alternative imaging technology to the spectral approach. Images are collected with a multiplanar [15] imaging system based on *en-face* OCT. This technology has been developed to simultaneously acquire *en-face* (C-scan) OCT images and corresponding confocal ophthalmoscopic images along with cross-sectional (B-scan) OCT at specifiable locations on the confocal image. Along with simultaneous confocal SLO imaging, the *eF*-OCT offers the possibility of multiple channels such as an additional one for fluorescence

imaging. Examples of images with pathology are presented here to illustrate the value of the *en-face* approach.

We take advantage of the OSA ISP software to present sets of such images which are displayed in 2, 3 or 4 C-scan images format, depending on the scanning regime and on the combination of imaging technologies. For instance, an *eF*-OCT/SLO system can generate simultaneously two images in the C-scan regime. The addition of a fluorescence channel in a three screen format is demonstrated along with a fourth screen which features a live mix of two of the other simultaneously working channels superimposed upon each other.

## 2. The OCT/SLO

Simultaneous acquisition of images in two channels, OCT and SLO requires configurations using splitters. A small fraction of the light returned from the retina is diverted towards the SLO channel using a separate splitter. There is an optimum splitting ratio which ensures sufficient and similar S/N ratio in both channels [16].

The main blocks of the *eF*-OCT/SLO system are shown in Fig. 1. The scanning procedure is similar to that used in any SLO system, where the fast scanning is *en-face* (line rate, using the scanning mirror MX) and the frame scanning is much slower (at the frame rate, using the scanning mirror MY) [17]. The MX mirror is driven with a ramp at 500 Hz while the MY mirror is driven with a ramp at 2 Hz. In this way, an *en-face* image in the plane (x, y) is generated at constant depth. The next *en-face* image at a new depth is then generated by altering the length of the reference path of the OCT interferometer, by controlling a translation stage in the reference path and repeating the (x, y) scan.

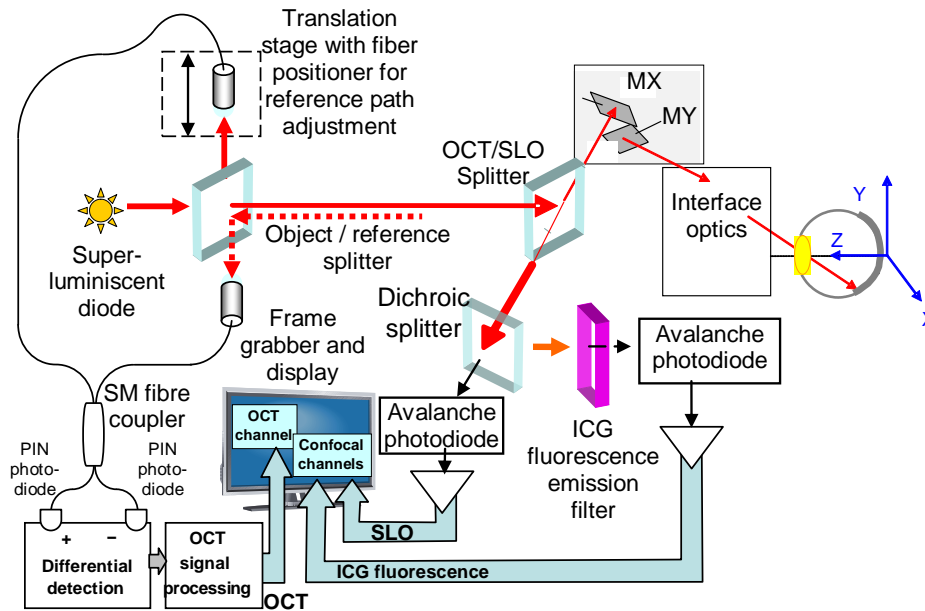


Fig. 1. Combined OCT/SLO system. MX, MY: galvanometer mirrors of the XY scanning pair. The confocal channels display a standard SLO image and an ICG fluorescence image (according to Section 3 below).

To construct B-scan images, the signal is interrupted to the MY mirror. The line scanner is driven with the same signal as in the C-scanning regime and the translation stage modifies the length of the interferometer arm continuously over the designated depth range in 0.5 s. In this case, an OCT cross-section image is produced either in the plane (x, z) or (y, z).

New imaging technology brings not only new information to the clinician, but with it, the requirement of interpretation. *En-face* OCT is no exception in this respect. The higher the depth resolution of the OCT system, the more fragmented the C-scan OCT image appears. The fragmentation is especially disorienting when the plane of the retina is tilted in relation to the scanning plane. First, the anatomic features of the *en-face* OCT image appear fragmented, making the image challenging to interpret. Second, variations in tissue inclination with respect to the coherence wave surface alter the sampling of structures within the depth in the retina, creating unbalanced distortions among the elements being sampled [18].

The most high reflective bright features in the OCT image occur at the intersection of the surface of  $OPD = 0$  with the tissue. Because of the particular way the retina is scanned, with the fan of rays converging on the eye pupil, the surface of  $OPD = 0$  is an arc circle with the center in the eye pupil. Depth exploration requires that the radius of the arc is altered. If the arc has a small radius, it may just only intersect the top of the optic nerve with the rest of the arc in the vitreous. The radius of the arc is changed by changing the length of one of the arms of the interferometer in the OCT channel to explore the retina up to the retinal pigment epithelium (RPE) and choroid. The plane of the retina tissue at the back of the eye is not flat and this complicates the interpretation of the sections of tissue in the images even further. Despite scanning images in an *en-face* plane, images may contain and include structures in depth similar to a B-scan OCT image. This effect is more prominent in high resolution *en-face* OCT [19], where the C-scan slices are very thin ( $3\ \mu\text{m}$ ).

These two effects, (i) fragmentation and (ii) multiple depths simultaneously displayed in the C-scan images are also present in images generated by high resolution confocal SLO systems, however at a scale where they are more easily ignored. In an SLO, the images do not appear fragmented and depth structures are barely visible due to the coarse depth resolution of  $0.3\ \text{mm}$ , grossly equivalent to maximal retina thickness in a normal eye. Fluctuations in focus adjustment produce a smooth transition from dark areas (low intensity signal) to bright areas (high intensity signal) in the image. The problems of interpreting *en-face* OCT images are largely the result of its high depth resolution and the mismatch of curvature between the scanning arc and the posterior curvature of the eye. Paired lower resolution SLO images, acquired and presented simultaneously provide orientation for the observer and help address the fragmentation problem.

### 2.1 Combination of OCT/SLO with fluorescence imaging

On one hand, indocyanine green (ICG) angiography and OCT appear well suited to operate together because they share similar spectral bands. The most widely used band for retinal OCT of the retina is  $820$  to  $920\ \text{nm}$  while ICG is usually excited at  $806\ \text{nm}$  and fluoresces in the band  $810$  to  $860\ \text{nm}$  with a peak at  $830\ \text{nm}$ . Operating in similar bands allows the same source to be used for ICG excitation as well as for the production of an OCT image. On the other hand, the proximity of the excitation wavelength to the fluorescence band raises several optimization issues. As it turns out, it would have been easier to combine OCT with fluorescein angiography, since the excitation wavelength and the fluorescence band are well separated. However, this would have required two separate optical sources [12].

The set-up of an *eF*-OCT system equipped with two channels, SLO and ICG fluorescence has been described before [20]. The OCT/SLO splitter used in the OCT/ophthalmoscope configuration in Fig. 1 to divert some of the light to a separate confocal receiver is replaced by a chromatic splitter. This separates the retina-scattered light at the excitation wavelength,  $792\ \text{nm}$  guided into the OCT channel, from the fluorescence signal, centered at  $830\ \text{nm}$ , guided towards the fluorescence confocal receiver. The residual transmission of the chromatic splitter (approx. 4%) at the OCT wavelength is sufficient to generate an SLO image. The fluorescence signal and the residual signal at the excitation wavelength are separated by a second chromatic splitter. To enhance the contrast of fluorescence in the confocal receiver, a supplementary filter "Fluorescence emission filter" is used in the fluorescence channel to

attenuate any excitation band light that gets past the two chromatic splitters. These are cold mirrors with a transition wavelength,  $\lambda_{tr}$  between the excitation band and fluorescence band. Superlum Moscow developed a comparatively powerful SLD for this project, with an output power of 5 mW ex fibre at  $\lambda = 792$  nm and  $\Delta\lambda = 21$  nm spectral FWHM which determines a depth resolution in the tissue in the OCT channel of less than 9  $\mu\text{m}$  (considering an index of refraction  $n \cong 1.4$ ).

### 2.2 Sequential imaging in C-scan and B-scan regimes

Current systems in ophthalmology now use spectral domain methods, based on either the Fourier domain OCT (using a line CCD camera [21]) or swept source OCT (using a tunable laser [14, 22]). Both are A-scan based systems and therefore the output image is a cross-section (a B-scan). C-scans can be generated by post-processing software from a stack of B-scan OCT images collected at different lateral positions from the retina volume.

In our system, both C-scan and B-scan images are hardware generated. Switching between the two modes is done by toggling a keyboard key. This facilitates a rapid alternation between firing sequences of *en-face* imaging (producing C-scans) and cross-sectional imaging (producing B-scans). This feature is not achievable in even the fastest research systems reported today using spectral domain OCT [14], because the collection of a whole volume still requires 1 second which is then followed by software slicing, i.e., to output a C-scan image takes over 1 second. In the current implementation described here, the frame rate is 2 Hz, i.e., a C-scan is produced in 0.5 s, in real time. Additionally, the SLO image in the OCT/SLO system, or the SLO image, fluorescence image and their combinations in the OCT/SLO/ICG systems are all produced in the same frame time of 0.5 s. The system could also operate at 4 Hz, with some reduction in the transversal resolution; however, all images presented have been obtained at a frame rate of 2 Hz. The transversal resolution determined by the number of pixels in the T-scans which are used to assemble B-scan and C-scan images is the same.

Due to the fact that both regimes use the T-scan mode (i.e., T-scans are used to assemble C-scan as well as B-scan images), this simplifies the software requirements and hardware demands of ensuring pixel-to-pixel correspondence between images generated in different regimes of operation.

The ease of switching between operation regimes helps to compensate for the lack of 3D imaging, now achievable in SD-OCT systems. At a rate of 2 Hz, eye movements deteriorate the images significantly and much more than in SD-OCT systems. Eye movement effects in B-scans are less present in SD-OCT images than in *eF*-OCT images, as SD-OCT systems can produce a B-scan at tens or even hundreds of Hz.

However, the effect of movement is more pronounced in the C-scan inferred image using SD-OCT because the time to acquire a whole volume of the retinal tissue is 1–10 seconds.

### 2.3 A fundus image in the OCT imaging of the retina

While the main motivation for providing a fundus image is to guide the imaging in the OCT channel, another reason is synergy in interpretation. Crucial for this operation is pixel-to-pixel correspondence between the two channels, OCT and fundus imaging. This can only be ensured if both channels share the same transverse scanner to scan the beam across the eye. Different possible generic configurations have been considered [12]. These show that the natural combination of the two channels would be that where the two images generated are both C-scans. This is the solution of choice embraced here.

A main advantage of *en-face* imaging is that it allows integration of SLO with OCT. This has proved useful in allowing ophthalmologists and vision scientists to associate features seen in confocal-SLOs and SLOs with *en-face* OCT images, fragmented due to the enhanced depth resolution. Such a method allows a dual presentation of high resolution images (OCT and SLO) in different regimes of operation, B-scan or C-scan, providing cross sections in depth or constant depth images respectively. Different solutions have been provided to

assemble OCT/SLO systems, depending on the scanning type and on the OCT regime of operation. We refer here to a system which can perform simultaneous OCT-confocal regime of operation. This allows imaging as a dual OCT/SLO, dual OCT/fluorescence imaging as well as triple OCT/SLO/fluorescence imaging. Different formats of displaying the images are possible. In the C-scan regime, two images are presented side by side. In the B-scan, either the B-scan image alone can be displayed on full screen, with the SLO image below on the side, or side-by-side in equal windows with the image provided by the SLO channel. In this regime the frame scanner is not driven and the image is absent but replaced by a mapping in the plane of lateral coordinate (usually X or Y) and time (usually along the vertical coordinate, replacing the frame coordinate of the previous C-scan image before switching the system to the B-scan regime. As the depth (along Z) is scanned at a constant speed, the time can be directly put in correspondence with the number of the line in the OCT B-scan frame and consequently with the depth value. The image generated by the SLO channel is a succession of the same T-scan repeated for each new line in the OCT B-scan. If the scanned eye is stationary during a B-scan, all T-scans are similar and show the same reflectivity pattern in successive lines, thereby forming an image of straight vertical stripes of varying brightness. If the eye moved grossly, these vertical stripes deviate from the vertical direction and may appear interrupted in the case of jerky movements. Most commonly, a 3-screen format is employed, displaying the SLO image obtained in the C-scan regime just before the OCT/SLO system was switched into the B-scan regime, plus the B-scan OCT image and the vertical lines tracings generated simultaneously in the SLO channel.

#### *2.4 Recognizable patterns*

Images from a diverse selection of patients from a large retina-specialty practice were studied with the dual channel OCT/SLO and correlated with clinical records. The standard protocol employed consisted of multi-slice sequences of dual-channel sets of C-scan OCT and corresponding confocal ophthalmoscopic images. Selectively targeted sequences of B-scan OCT were also acquired.

The research reported here was conducted under the tenets of the Declaration of Helsinki, informed consent was obtained and the nature and possible consequences of the study were explained.

Advantages of the simultaneous OCT/confocal acquisition have been discussed [12, 15, 23] and several remarkable new aspects of clinical anatomy were revealed using this new perspective. The versatility of selective capture of C-scan OCT images and B-scan OCT images at precise points on the confocal image affords the clinician a more complete and interactive tool for 3D imaging of retinal pathology.



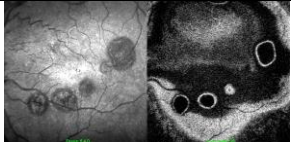
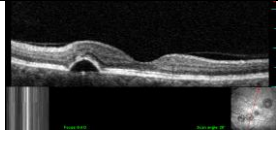
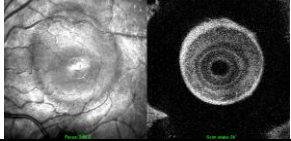
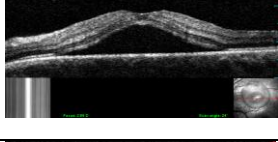
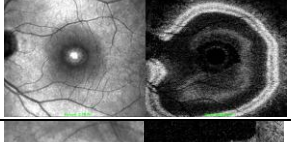
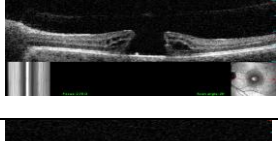
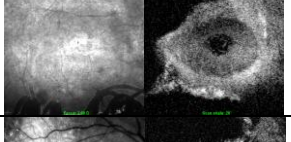
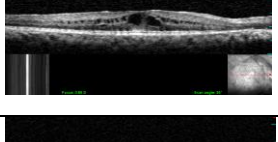
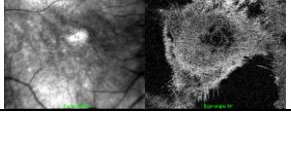

Disease	Pattern	C-scan OCT/SLO Image	B-scan OCT image
RPE detachment	Rings of light (isolated bright circles surrounding dark spaces)		
Central Serous Retinopathy	Bullseye target (concentric rings of alternating bright and dark lines)		
Macular hole	Petaloid wreath (ring of cysts around a central axis)		
Cystoid macular edema	Swiss Cheese Wheel (cluster of circular holes)		
Epiretinal membrane	Shining star (radiating lines)		

Fig. 2. Association of patterns provided by C-scans and B-scans with different diseases.

After examining a diverse array of common clinic pathologies a series of specific and reoccurring patterns became evident. Observation of uniquely specific and reoccurring patterns for several pathologic entities is possible in the *en-face* display only. The table in Fig. 2 reviews some of the most common patterns. The different observed patterns strongly depend on the imaging depth position; however, they were consistently obtained by recording many C-scans while the operator scanned the depth manually.

Associated B-scans, obtained by switching the OCT/SLO system into the B-scan regime, are also shown. In all images in the extreme right column, the insets below the B-scan image represent the SLO images just before the OCT/SLO was switched from the C-scan to the B-scan regime (right) and after the switch, when the OCT/SLO operates in the B-scan regime (left). This is why the image in the left inset displays vertical stripes only, whose alignment enables a determination of the extent of the lateral movement of the eye during the 0.5 s in which the B-scan was acquired. This will be documented in more detailed below.

### 2.5 Comparison of T-scan based OCT systems with A-scan based OCT systems

SD-OCT systems are A-scan based. B-scan images are assembled from A-scans. An equivalent SLO image can be generated from collecting several OCT B-scans sampling the tissue volume. Then, by software means, an SLO image can be reconstructed without using a beamsplitter or a separate confocal receiver. Both OCT and the reconstructed SLO image are obtained via the same aperture optics. Such an equivalent SLO image is obtained only after all the images in the stack have been acquired. Therefore, such a method is suitable only for use with fast OCT systems, such as SD-OCT. With a high density of 50–100K A-scans, obtained at tens of kHz, a few seconds are required for the whole volume. Such a method has been demonstrated using both SD-OCT methods, FD-OCT and SS-OCT. After a 3D data set



acquisition, an SLO-like image is generated and then the B-scan OCT images can be revisited through the 3D data set with simultaneous display of the synthesized SLO image. Several groups have reported reconstruction of an SLO-like image from B-scans using FD-OCT systems [21]. A feature-based algorithm [24] which can register a high density OCT image of the fundus image from normal density scans was developed. The main advantage of the method relies on the speed of SD-OCT which allows collection of a large data set of pixels in a minimum of time.

A similar procedure has been applied to generate an SLO-like image from a stack of SS-OCT images acquired with systems operating at 850 nm [25] and at 1  $\mu\text{m}$  [26].

While the pixel-to-pixel correspondence is ensured, such a method presents the following disadvantages:

(a) For A-scan based OCT systems, the time to collect the whole volume of voxels determines the time required to produce a C-scan image,  $T_{en-face}$ , since such an image is only available once all data has been acquired. Progress in mode locked SS-OCT lead to a  $T_{en-face}$  time of less than 1 second which becomes useful in practice. However, even if the progress was substantial in the last few years, this value is still more than an order of magnitude larger than the time to produce a C-scan image using an *eF*-OCT system equipped with resonant scanners [13].

(b) In addition, the transversal resolution along the synthesis axis of the SLO image is given by the spatial sampling, i.e., by the lateral interval from a B-scan to the next B-scan along a direction orthogonal to that contained in the B-scan image. Such SLO-like C-scan images exhibit the normal transversal resolution (15-20  $\mu\text{m}$ ) along the B-scan lateral coordinate (X) but a coarser sampling interval, along the lateral rectangular direction (Y). This size could be reduced by increasing the acquisition time in order to capture more B-scan images but would also result in more cumulated artifacts due to movement.

## 2.6 Correction of the C-scan and B-scan OCT images based on the information collected from the simultaneous SLO channel

The simultaneous OCT/fundus imager permits some eye movement correction using the signal in the fundus (SLO) channel. The design ensures a strict pixel-to-pixel correspondence between the two C-scan images, OCT and SLO. This helps in two respects:

(i) For small movements, the SLO image can be used to track the eye movements between frames and for subsequent transversal alignment of the OCT image stacks [11]. For large movements and blinks, the SLO image gives a clear indication of the OCT frames that need to be eliminated from the collected stack. As a reference for the aligning procedure, the first artifact-free confocal image in the set is used. This is illustrated in Subsection 3.2.2 below.

(ii) In the B-scan regime, movements of the eye are indicated by lateral shifts of the confocal traces. With the OCT/SLO operating in the B-scan mode, each horizontal line in the SLO image has a counterpart line in the OCT image that corresponds to a depth position. The relative lateral eye movements lead to slight deviations of contours in the SLO image which can be employed to correct the lateral shift of the lines in the B-scan OCT image (such contours are illustrated here in left insets below the B-scan OCT images in the table in Fig. 2). This procedure is described in the Subsection 3.5 below.

## 2.7 Performing SLO first

It is advantageous to perform fundus imaging first to guide the investigation. Combining the OCT and SLO techniques allows correlation of information in orthogonal planes and facilitates more accurate diagnosis. Previously, we illustrated a classic example [12] where B-scan images of the retina did not show any signs of abnormality. Since the slice was collected as the patient was instructed to fixate on a specific target, the image captured was a cross-section of the macula which was spared, where the visual acuity was best. The report sent to the clinician was that the macular anatomy of the patient was normal. Subsequently, when an

additional study was performed using the OCT/SLO, the SLO image revealed a slightly eccentric perifoveal disturbance. The *en-face* perspective was able to more accurately redirect the investigation. When the OCT/SLO was switched to the B-scan regime, the cursor line was placed over the position in question, revealing an RPE cystic lesion.

Performing SLO first is not currently possible with the SD-OCT systems. If a feature is noticed in the C-scan reconstructed image at the end of the acquisition process, then this may require acquisition of another set of B-scans to generate a more accurate 3D volume.

### **3. *eF*-OCT/SLO/ICG functionality**

Using the OSA ISP software, we illustrate the functionality of the *eF*-OCT/SLO/ICG system in terms of correlation of information between the images displayed, as seen live while investigating the patient. The images are 12-bit grayscale and they are displayed simultaneously. Two formats were possible, of either side-by-side, three on a screen, or alternatively along with a fourth channel which displays the real-time overlay of the ICG image on the C-scan OCT image.

#### *3.1 Polypoidal choroidal vasculopathy*

Figure 3 demonstrates the utility of the system in evaluation of a retina of a patient with polypoidal choroidal vasculopathy, an unusual variant of neovascular macular degeneration. X-Y *eF*-OCT images are shown and light-box displays. A set of 116 images were acquired in 58 seconds. 20 images were removed due to blinks and movement effects.

##### *3.1.1 X-Y sections (C-scans)*

Coronal sequence at 2 frames per second following ICG injection are presented in Fig. 3(a). The ICG angiography images reveal a leash of abnormal vessels which originate near the nerve, extend infero-temporally, and terminate with bulbous endings. The accompanying OCT images capture the sausage-shaped cuff of fluid surrounding the vessels which accounts for the lumpy polypoidal appearance in the SLO images in the upper left quadrants of the display. The overlay channel at the bottom right of the 4-image panel, displays the relationship between the vascular structures and the anatomic effect of the fluid leakage by revealing the vessels within the core of the resulting RPE elevations. While the pixel-to-pixel correspondence of the matching images ensures that the locations in each image are in proper registration, the delays in scanning from top to bottom create the appearance of back and forward tilting of the images when the sequence is played as a movie. The images of Fig. 3 show little movement artifact owing to the patient's good fixation ability. There is still some tilting appearance due to the time between the capture of the upper and lower portions of the images.

##### *3.1.2 Light-box*

As shown in Fig. 3(b), this displays 4 sequential 4-image frames and is useful in reviewing the progress of the ICG 4 frames at a time. This feature is illustrated for this case only to demonstrate the OSA ISP capability. It could have been equally applied to all the subsequent cases presented below.

##### *3.1.3 B-scan regime*

The eye has moved axially and transversally, as shown by distortions of the C-scans. Sections X-Z and Y-Z and the volume displays, provided by the OSA ISP software are not useful for these data sets. Therefore, the only way to generate a meaningful B-scan OCT image is by switching the system into the B-scan regime. This is a unique feature of the *eF*-OCT, both C-scan OCT and B-scan OCT images are generated by hardware means, i.e., the OCT channel acquires and generates the OCT image in real time. This allows sequential switching from C-

scan to B-scan and back as mentioned in Subsection 2.2 above. Such a procedure is not feasible with SD-OCT as acquisition and software steps are required, which take time.

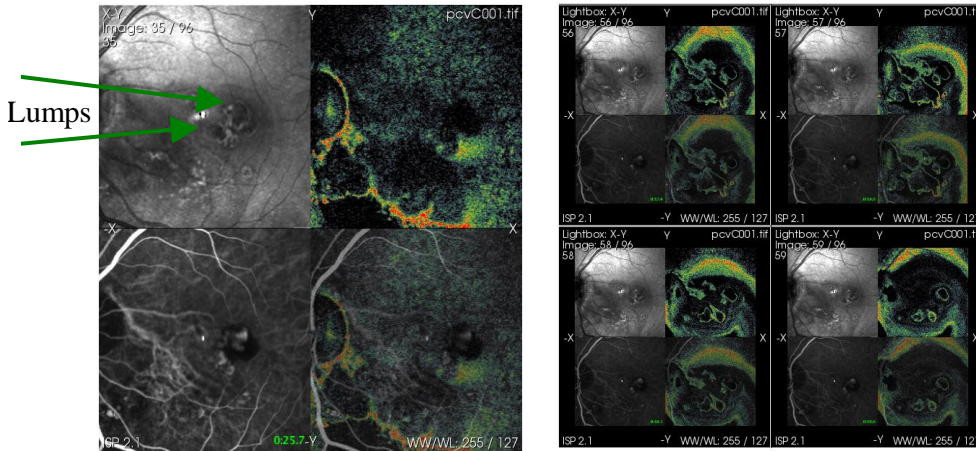


Fig. 3. 96 4-C-scan ICG/OCT/SLO sets of a patient with polypoidal choroidal vasculopathy. (a) XY display (View 1); (b) Light-box display (View 2). The SLO image in the upper left of each 4-up C-scan appears thickened with a lumpy, multi-lobular or “polypoidal” texture to the surface of the retina, as shown by the arrows. (Counter 15 s on the ICG image): Early arterial phase of ICG sequence reveals abnormal choroidal vessels. OCT depth is within the choroid and shows evidence of shadowing. (Counter 28 s on the ICG image): Mid arterial-venous phase demonstrates a leash of deep abnormal vessels with hyper-fluorescent bulbous endings. OCT image outlines the overlying serous elevation surrounding the vessels and hot spots. (Counter over 1 minute on the ICG image): Full venous phase of the ICG angiogram shows increased leakage at vessel endings. The OCT reveals the outlines of the serous cuff around the vessels and enlarging fluorescence accumulations. In all C-scan images, lateral size is 22°x22°.

Figure 4 shows the display in the B-scan regime, for several instances between 2 minutes and 40 seconds and 3 minutes and 25 seconds following the injection. The C-scans on the left were the images collected in the SLO and ICG channels immediately prior to switching the instrument to the B-scan regime. The lateral size in the B-scan regime is the same as that of C-scan images while the vertical axis is oriented along the depth coordinate. The expanded vertical appearance of the B-scan image is due to placement of the B scan adjacent to the corresponding C-scan within the confines of the monitor geometry. While this presents a somewhat exaggerated stretching of the vertical dimension, the users found this preferable to a compressed appearance which would result if the true more horizontally-biased aspect ratio of the B-scan OCT were maintained. While the stretching exaggerates some features, it allows the user to see more details within the retina than are visible if the image were confined to its true aspect ratio.

The lumpy polypoidal appearance is further investigated in the wide-view versions of B-scan OCT images as shown in Fig. 5. The B-scan is displayed along the screen and the two C-scans in Fig. 4 are now displayed underneath. These wide views of the B-scans provide a more accurate image of the choroidal polypoidal lesions distorting the RPE profile and the associated overlying subretinal fluid. The elevation on the right shows evidence of vascular invasion into the overlying retina.

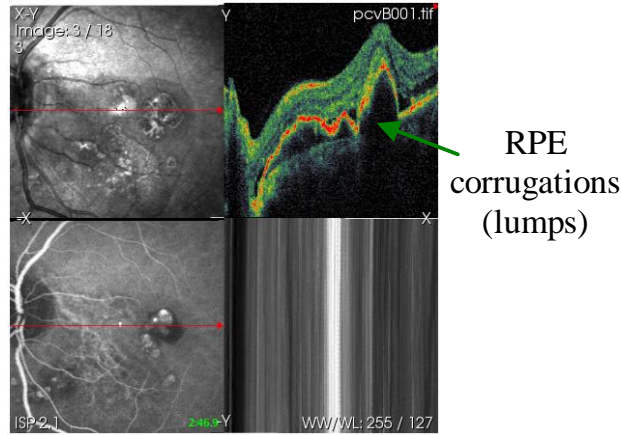


Fig. 4. ICG/OCT/SLO sets of the same patient as that in Fig. 3 (with polypoidal choroidal neovascularization). 18 B-scan OCT images (View 3) are collected for 7 different orientations of the red line projected over the ICG image, through different areas of leakage: images 1, 2, 3, 14 and 15 (1st orientation), images 4 and 5 (2nd orientation), image 6 (3rd orientation), images 7, 8 and 9 (4th orientation), images 10, 11, 12 (5th orientation), image 13 (6th orientation) and images 16, 17 and 18 (7th orientation). The OCT reveals corrugated elevation of the RPE. The straightness and the verticality of the lines in the images provided by the SLO channel in the lower right frame confirm good alignment with minimal movement artifacts. The Z-axis (according to Fig. 1) of the B-scan (vertical Y axis in the display) is expanded by the horizontally confined configuration of the multi-channel display producing a vertical exaggeration of the aspect ratio. C-scan images: lateral size is  $22^\circ \times 22^\circ$ . B-scan OCT image: lateral size (horizontal) is  $22^\circ$  and 1.3 mm in depth (vertical, measured in air).



Fig. 5. Wide display of B-scan images in the B-scan regime, for the same patient as that in Fig. 3 (with polypoidal choroidal neovascularization). 6 B-scan OCT images (View 4) are collected for 3 different orientations of the red line projected over the SLO image (bottom right). Images 1, 2 and 6 (1st orientation), images 3 and 4 (2nd orientation) and image 5 (3rd orientation). The inset underneath the B-scan image on the right displays the C-scan just before switching the systems from C-scan to B-scan. The SLO image in the inset underneath on the left is the image generated by the SLO channel in the B-scan regime. B-scan OCT image, lateral size  $22^\circ$  and 1.3 mm in depth (measured in air).

Once such an OCT B-scan is obtained, it can be viewed as a 3-dimensional intersection of orthogonal planes at its origin on the corresponding C-scan OCT, SLO or ICG (SLO) image, as shown in Fig. 6. The OCT cross-section shows the multiple underlying disturbances in the RPE which have produced elevation on the retina and pockets of subretinal fluid. The ICG images show the fluorescence of the contrast dye filling the normal and pathological vessels. This cross-planar view allows the observer to appreciate the critical spatial relationships between the features visible in the *en-Face* perspective (i.e., vascular leakage pattern) and the anatomic changes (i.e., retinal elevation) in the Z-axis .

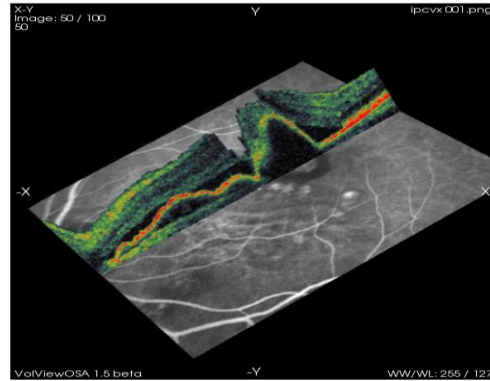


Fig. 6. B-scan OCT at its origin on the ICG image ([View 5](#)) for the same case of polypoidal choroidal neovascularization in Figs. 3 to 5.

### 3.2 Case of recurrent choroidal neovascularization in age-related macular degeneration

A second case is that of recurrent choroidal neovascularization in wet age-related macular degeneration which had been previously treated with focal laser photocoagulation.

#### 3.2.1 X-Y sections (C-scans)

119 images have been collected in 60 seconds. 32 images, showing blinks and large movement distortions have been eliminated. During this time, the operator has manually scrolled the depth from just in front of the retina to the choroid, several times.

The upper left panel shows the confocal SLO image which highlights a bright area representing an atrophic scar above the infero-temporal arcade. On the foveal side of the scar, a dark lesion is seen surrounded by concentric alternating halos of light and dark. A similar pattern is seen in the upper right panel which displays a coronal OCT slice through the macula. The bright outer rings, seen best superiorly represent the RPE. The internal rings are inner retinal layers, with the innermost bright circle being the retinal nerve fiber layer. Internal to it is a black ring which represents the vitreous which surrounds the central elevation which is an active choroidal neovascular hemorrhagic mound. The lower left panel displays the vascular filling sequence of ICG dye illuminating the choroidal and retinal vessels. By scrolling through the stack using the left cursor, the temporal sequence of ICG filling is revealed. An irregular vascular formation is seen extending from the atrophic area towards the fovea. It is surrounded by a dark halo which protrudes above the surface of the macular bowl and probably consists of fluid and blood.

The spatial overlap between the vascular events and the surface topography is revealed by the active overlay channel in the panel on the lower right. In order to avoid missing the early filling sequence the timer and image recording were initiated at the completion of the injection. Transit time to the eye typically takes 10 to 12 seconds but may vary between individuals due to differences in circulation.

### 3.2.2 Correcting the eye movements in the C-scan OCT image and in the ICG image using the information in the SLO channel

Inspection of the cross section cuts in the images above show that during the one minute session, the eye has moved axially by more than 4 times the retina thickness. Therefore, X-Z, Y-Z sections and volumes are not shown. The eye has also moved considerably sideways. On the same case we demonstrate the capability of the OCT/SLO system of using movement information from the SLO channel to correct for the OCT channel [11]. We then illustrate the capabilities of the OSA ISP software on such a set of transversally aligned 4-up images in Fig. 8(a). We selected the first 36 images of the set in Fig. 7 which corresponds to operator controlled scanning in depth from the top of the retina to the choroid. We have retained images which did not show obvious and large movement effects. (In fact, they are all affected by some movement at a close inspection). We then aligned the remaining images in the set transversally using the lesion shown as a bright patch in the centre of the SLO image on the top left of the X-Y display in Fig. 7.

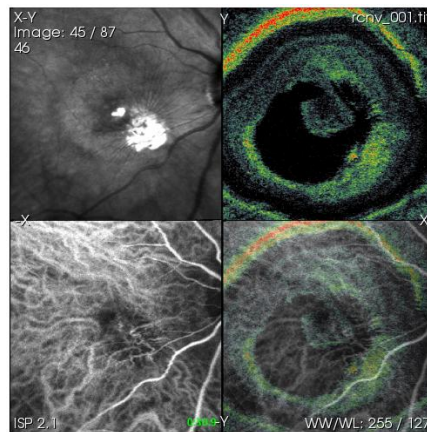


Fig. 7. 4-up image display of scans acquired in the first 1 minute from a patient with recurrent choroidal neovascularization (View 6). X-Y: Each image in the panel captures the same 29 degrees, since only one scan is actually performed with feeds to 3 separate channels. The panel seen in the lower right of the 4-up is a mixture of the ICG channel (lower left) and the C-scan OCT (upper right). The ICG sequence shows the contrast dye enters the normal vessels and the abnormal nest of choroidal neovascularization at the edge of the old laser scar.



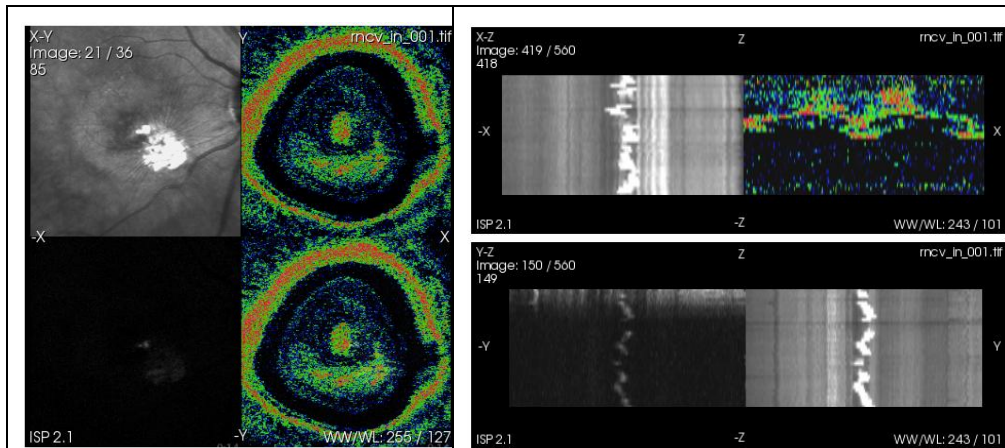


Fig. 8. For the same patient as in Fig. 7, illustration of the eye movement correction of the C-scan OCT images and of the ICG images using the information in the SLO channel in (a) and validation of this correction on the inferred B-scan images in (b). (a) X-Y display: by scrolling the cursor through the 36 images it can be noticed that the retina features are stable transversally, the bright lesion is fixed while the small bright patch corresponding to the interface optics stray reflection oscillates transversally (View 7); (b) X-Z (top) and Y-Z (bottom) display: traces of the retina are now vertical. Image 420 in the X-Z sequence and image 149 in the Y-Z sequence show cuts through the interface optics stray reflection. Their wavy contours display the eye movement in the X-Z and in the Y-Z plane, respectively (View 8).

Image sets were aligned using translation, so that distances between any pair of points remained unchanged. For the 4-up image sets, the SLO dataset was aligned, the same translation then applied to the datasets of the other channels, OCT, ICG and the overlay, and a composite stack reassembled. After alignment, the SLO images display a stationary image of the lesion while it can be seen that reflex from the lenses in the interface optics which usually aligns with central fixation bounce around as the sequence of frames are scrolled through using the OSA ISP software. The alignment retained the central part of images of size 280x280 pixels out of the original 303 x 303 pixels set. The images in Fig. 8(b) illustrate the X-Z-sections and Y-Z sections in the stack of 36 aligned C-scans. The quality of alignment is demonstrated by the verticality of traces corresponding to reflections from the retina in the SLO image. For instance, these traces can be checked on the X-Z cuts by scrolling the value of Y through pixel values beyond the middle of the set of 4-up C-scan images (280) to intersect the SLO image on the left. Cuts through the SLO images are seen on the left and cuts through the C-scan OCT images are seen on the right. Slices around number 418 display the wavy form of the reflex from the interface optics. Similarly, traces from the retina can be watched on the Y-Z cuts by scrolling the value of X through pixel values before the middle of the set of 4-up C-scan images (280) to intersect the SLO image on the right. Cuts through the SLO images are seen on the right and cuts through the ICG image are seen on the left (these do not intersect any features in the set of 36 images). Slices around number 149 display the wavy form of the reflex from the interface optics.

Figure 9 displays comparisons of X-Y cuts and Y-Z cuts in the original set in Fig. 7 with corresponding cuts in the aligned set in Fig. 8(a). The images in Fig. 9 do not bear any imaging information. The goal here is not to illustrate B-scan inferred cuts, but instead to demonstrate that we can trace the transversal movement of the eye by inspecting the information provided by the SLO channel and even more, that we can use such information to correct the C-scan OCT images for transversal movement. The X-Z cuts offer information on the lateral eye movement along X while the Y-Z cuts offer information on the lateral eye



movements along Y during the acquisition of the stack of OCT C-scan images. From frame to frame, the eye has moved laterally and traces in the SLO images are irregular (as shown in (a) and (c)). In (b) and (d), the traces are vertical, proving the efficiency in aligning the images transversally. The correction is applied to each frame to be moved laterally to the correct place. This makes the tracked features coincide, while the reflections from the interface optics will provide information on the movement. This is clearly illustrated by the reflection from one of the lenses in the interface optics (IO) in (b) and (d) which oscillates left and right while the other traces, from the tissue are well aligned vertically.

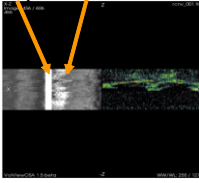
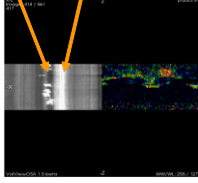
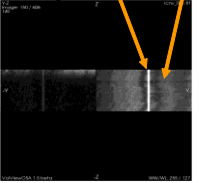
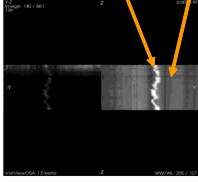
			
<p>(a) X-Z section in the set in Fig. 7 across the interface optics (IO) reflection and a bright part of the lesion. The vertical traces from the lesion and retina are irregular due to the lateral eye movements along X during the 18 seconds acquisition time of 36 of 4x C-scan images.</p>	<p>(b) X-Z section in the aligned set in Fig. 8(b), across the interface optics (IO) reflection and a bright part of the lesion. The IO reflection trace shows the movement of the eye along the X direction during the 18 seconds acquisition time. All other traces are from the retina and they are vertical, including that of the bright part of the lesion.</p>	<p>(c) Y-Z section in the set in Fig. 7 across the IO reflection. The vertical traces from the retina are irregular due to the lateral eye movements along Y during the 18 seconds acquisition time of 36 of 4x C-scan images.</p>	<p>(d) Y-Z section in the aligned set in Fig. 8(b), across the IO reflection. This shows the movement of the eye along the Y direction during the 18 seconds acquisition time. All other traces are from the retina and they are vertical.</p>
<p>The images are X-Z cuts beyond the middle of the set of 4-up C-scan images to intersect the SLO image on the left. Left, X-Z cut in the SLO images; Right, X-Z cut in the C-scan OCT images.</p>		<p>The images are Y-Z cuts beyond the middle of the set of 4x C-scan images to intersect the ICG image on the left. Left, Y-Z cut in the ICG images; Right, Y-Z cut in the SLO images.</p>	

Fig. 9. Comparison of B-scan inferred traces in the stacks of C-scan images in Figs. 7 and 8, illustrating the capability of detection of lateral eye movements using the SLO image, and the possibility of using such information to align transversally all the C-scan images in the 4-up display. The depth axis is oriented upwards in all images.

The alignment can be checked on the X-Z and Y-Z cuts, best by scrolling the images beyond the middle of the stacks, to skip the overlay channel. For instance, by scrolling beyond number 280, the X-Y cuts intersect the SLO image on the left and the C-scan OCT on the right. The bright lines are almost vertical proving the quality of transversal adjustment.

The X-Z and Y-Z cuts in the 3D volume are not however useful due to the reduced number of slices (36) and axial eye movements. This is a problem for the TD-OCT where the SD-OCT methods prove their superiority. We illustrate the alignment only on this case in this report and we have not attempted to produce volumes in the presentation of any patients.

### 3.2.3 B-scan regime

Even after transversal alignment, the cross section OCT images in the stack are distorted due to axial eye movement during the stack acquisition. In principle, this can be improved using an axial tracker [27]. The only way to compensate for the lack of the volume analysis is in this case the fast sequential short alternating sessions in the C-scan and B-scan imaging. The

switch is practically instantaneous, and is accomplished with the toggle of a key. Therefore, the system is switched into the B-scan regime and several such 4-up combined images are shown in Fig. 10. The images in the left column are SLO and ICG images collected in the C-scan regime just before switching the system into B-scan regime, to obtain the images displayed in the right column, top in the OCT channel and bottom, provided by the SLO channel. Figure 10 shows 34 such selected images, with little effect of the eye movement, monitored by the traces in the SLO channel images, bottom right.

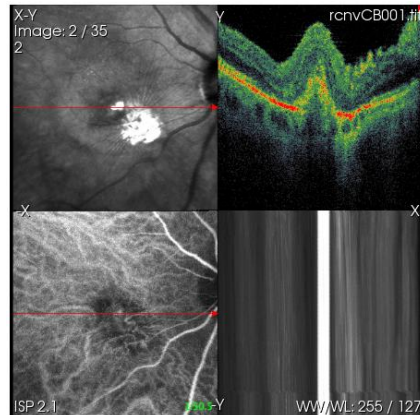


Fig. 10. Panel of 4 images generated in the B-scan regime (View 9) for the same patient as that in Fig. 7 (with recurrent choroidal neovascularization). 34 images made of two C-scans (left column) and the pair of images OCT/SLO in the B-scan regime (right column), following a 1st image in the set which is a 4-up all C-scan images. The system has been switched into the B-scan regime at 1 minute 50 seconds after the ICG injection, starting with the image number 2. The B-scan OCT in the upper right panel reveals a corrugated inner retinal surface due to cicatricial contraction from the previous laser treatment. The lower left panel shows retained ICG dye in the vessels and some leakage at the site of the membrane. The spatial limitations imposed upon the aspect ratio due to the 4-up display results in compression of the horizontal dimension producing a somewhat exaggerated vertical appearance of the cross-sectional features of the B-scan. The frame in the lower right shows the lateral movements during the acquisition of the B-scan OCT. Note the lateral shifts in vertical lines.

### 3.3 Central Serous Retinopathy (CSR)

#### 3.3.1 X-Y sections (C-scans)

Figure 11 shows a CSR case, for which 120 C-scan images were collected in 60 seconds. Only 100 images were retained, after images with serious blinks and movement distortions were eliminated. The eye was left drifting axially and therefore C-scans at different depths are collected. The upper left image displays an irregular retinal surface disturbance highlighted by the gray-scale of the confocal SLO. Underlying the surface, multiple RPE detachments are seen as bright rings in the C-scan OCT in the upper right panel. The ICG sequence in the lower left shows an absence of associated focal leakage suggestive of CSR. Confirmation of the lack of connection between the vascular sources for the RPE detachments (which would indicate choroidal neovascularization as their etiology) is visually suggested by the overlay channel in the lower right. The three live C-scan frames and the overlay image all move in synchrony slightly back and forth with the patient's microsaccades. At each frame, however, the images correspond perfectly transversally.

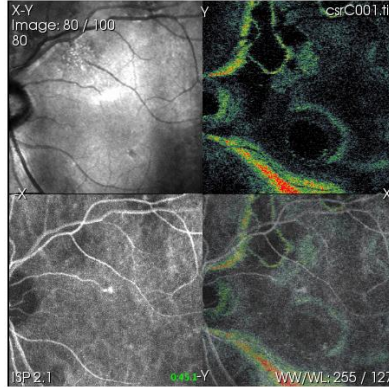


Fig. 11. CSR case, first phase, up to 59 seconds ([View 10](#)).

### 3.3.2 B-scan regime

After switching the system into the B-scan regime, a 4-up image set presentation is produced as shown in Fig. 12. The cross-section reveals the relationship of overlying serous fluid to the RPE detachments at the level of the red line shown in the frames on the left. A boggiess of the overlying retina is also evident in the B scan frame. The 4-up display compresses the horizontal expanse of the B-scan exaggerating the z-axis and making the retinal appear thicker than it really is.

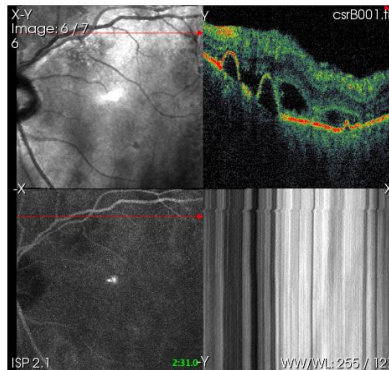


Fig. 12. Display of 4 images in the B-scan regime ([View 11](#)) for the same patient as that in Fig. 11 (CSR case). 7 images are shown obtained for three different positions of the red line over the ICG image in the bottom left. Image 1 (for the 1st position), images 2, 3 and 4 (2nd position) and images 5, 6 and 7 (3rd position).

Figure 13 illustrates a different presentation of images in the B-scan regime, where the B-scan is allowed to expand to the maximum width allowed by the display. Underneath the B-scan OCT image are the simultaneous SLO image on the left and the SLO image recorded immediately before switching the system to B-scan mode on the right. This display presents a more accurate impression of correct aspect ratio and reveals more details of the internal retinal features.

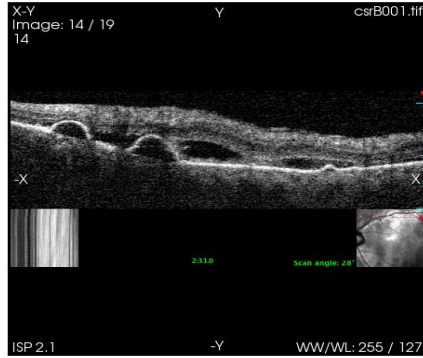


Fig. 13. The same case of CSR in Figs. 11 and 12. Display of 22 B-scan images obtained in the B-scan regime (View 12) for six different positions of the red line oriented horizontally over the SLO image in the bottom right inset. Images 1 and 2 (1st position), images 3-8 (2nd position), image 9 3rd position), image 10 (4th position), images 11 and 12 (5th position) and images 13-19 (6th position).

### 3.4 Diabetic retinopathy

A case of diabetic retinopathy is shown in Fig. 14. C-scans from the First 40 seconds following ICG injection reveal a granularity to the internal retinal layers while the ICG highlights focal collections of dye in small microaneurysms. 67 images are retained out of 80, after eliminating those with blinks and serious distortions due to the eye movement. Several 4 up C-scan images after 1 minute are also included by the end. X-Y cuts have been selected as for the previous illustrated cases. The OCT C-scans demonstrate subtle tilting of the eye which is not evident on the matching SLO scans which have lower axial depth resolution. In the lower part of SLO image, the patient's lashes are evident, indicating his tendency to close the eye which produces some upper rotation. This rotation is only minimally evident on the SLO as a softening of the focus of the inferior part of the SLO and ICG frames, while on the OCT C-scan it produces a black patch on the bottom of the image.

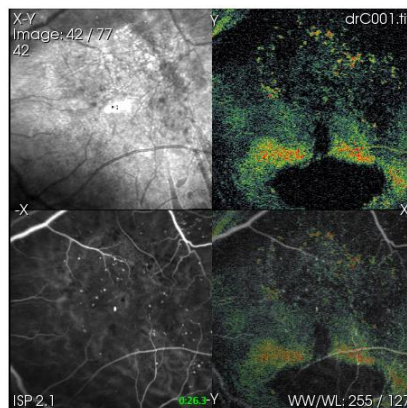


Fig. 14. 4-C-scan images of a patient with diabetic retinopathy (View 13).

B-scan images presented in Fig. 15 reveal a small foveal serous detachment which is typically unrecognizable by fluorescence imaging due to lack of any characteristic leakage pattern.

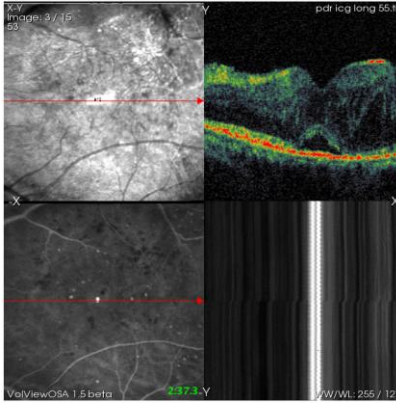


Fig. 15. ICG/OCT/SLO sets of a patient with diabetic retinopathy in the B-scan regime. 16 B-scan OCT images (View 14) are shown, collected after 2 minutes 40 s for 4 different orientations of the red line projected over the ICG image. Images 1, 2 and 3 (1st orientation), 4, 5, 6 and 7 (2nd orientation), images 8, 9, 14, 15 and 16 (3rd orientation) and images 10 to 13 (4th orientation).

Wide-view B-scan images presented in gray scale in Fig. 16 reveal a more subtle elevation of the fovea and some edema residues (hard exudates). Here the retinal edema appears less exaggerated but more characteristically thickened.

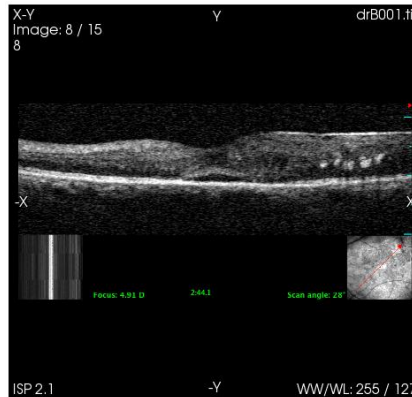


Figure 16. ICG/OCT/SLO sets of a patient with diabetic retinopathy. 15 B-scan OCT images (View 15) are collected at different moments after 2 minutes 40 s for 4 different orientations of the red line projected over the ICG image. Images 1-7 (1st orientation), images 8-11 (2nd orientation), images 12-15 (3rd orientation).

### 3.5 Correcting the eye movements in the B-scan OCT image using the information in the SLO channel

We now illustrate the other capability of the dual system mentioned above, that of aligning lines within the B-scan OCT images using the information provided by the SLO channel. During the acquisition of a B-scan, the SLO channel provides a repetition of T-scans at different times. The T-scan consists in a variation of reflectivity depending on the transversal coordinate. For a steady eye, the bright and dark features should determine bright and respectively dark traces along the vertical of the B-scan image. If a lateral movement has taken place, then the corresponding T-scan will show a lateral shift in the succession of bright and dark features. The number of the T-scan line within the SLO image corresponds to a

certain time within the frame interval of acquiring the OCT B-scan, i.e., the same number T-scan in the OCT image suffered the lateral shift too. Therefore, information in each T-scan in the SLO channel can be fed to the corresponding T-scan in the B-scan OCT image. For aligning SLO line scans, the smallest measurable difference between two neighbouring lines was determined. Then, the corresponding line in the OCT B-scan image was shifted laterally by the same amount in the opposite direction. This corrects for the effects of the eye movements projected along the x-axis. ImageJ, with the TurboReg plugin [28] in Batch mode (using a mask), and custom-written MATLAB [29] (version R2008a) code were used.

Such a correcting modality is illustrated in Fig. 17 for a polypoidal choroidal vasculopathy and for a diabetic retinopathy case. The correction is not perfect because the lateral shift is along a direction which goes out of the XZ plane. The correction can only amend the effect of the projection of the deviation due to movement into the XZ plane.

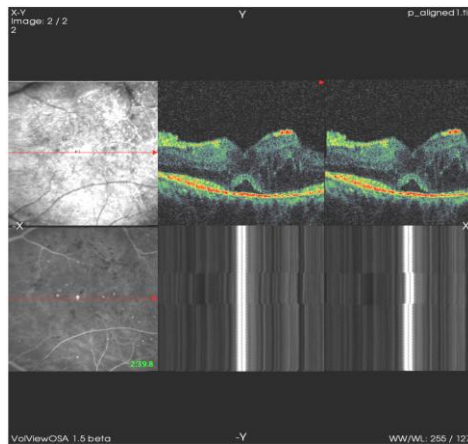


Fig. 17. The images on the left show the SLO (top) and ICG image (bottom) just before the system was switched into B-scan regime. The columns in the middle represent instances where the eye has moved laterally while collecting the B-scan image (top) as shown by the jaggedness of the vertical bright traces in the SLO image (bottom). Corrected B-scan OCT images are shown in the next column, where the bright traces underneath show the effect of the alignment by being moved in the opposite direction. Two sets are shown (View 16), for a polypoidal choroidal vasculopathy (1st set) and for a diabetic retinopathy case (2nd set).

#### 4. Discussion

The future of ophthalmic imaging lies in the integration of different types of information synthesized from combinations of techniques. The multi-modal functional imaging concept holds the promise of earlier and potentially more sensitive detection of retinal pathologies, as well as a better grasp of their pathogenesis.

Due to the limited acquisition rate of TD-OCT, the images are affected by movement so much so that the volume function of the OSA ISP software was not applicable to our sets. The B-scan images inferred from a set of C-scan images, even after transversal alignment had limited clinical values due to the small number of slices and axial movement artifacts. However, in real-time, the system can be easily switched to the B-scan regime where it provides a high quality cross-sectional OCT image, of comparable quality to A-scan based TD-OCT systems. This can be superposed over an SLO image, hardware obtained, as shown in Fig. 6. This SLO image presents better transversal resolution and has less movement artifacts than the fundus images currently inferred from SD-OCT stacks.

We have demonstrated the simultaneous operation of two separate channels (OCT and SLO) and three separate acquisition and display channels (OCT, SLO and ICG fluorescence) in a T-scan based retinal imaging system. We have also shown the utility of displaying a



mixer channel which can controllably mix the OCT and the ICG information (both C-scans). The pixel-to-pixel correspondence inherent in the design of this system allows an integrated and potentially more accurate analysis of the association between morphology and function within the retina and choroid than is currently possible with separate instruments. In these images, blood vessels are well-defined in the ICG images while incompletely revealed within the OCT images. At the same time, the depth resolution in the ICG channel is orders of magnitude lower than the OCT axial resolution and morphology cannot be assessed accurately. Therefore we believe that such a system can have valuable applications by combining the complementary information supplied by the two data channels. Regions of leakage, visible in the ICG image can be selectively examined in depth by acquiring B-scan cross-sections in the OCT channel.

Speed of acquisition with this system, while adequate for most patients, was a limitation for some of our more difficult cases. Control of movement artifact is, of course, a primary attraction to spectral-domain based OCT instruments.

The compound information acquired with a combined OCT/SLO/ICG instrument is able to benefit from good penetration into the choroid in the fluorescence channel, which should complement the OCT imaging of the deeper sub-RPE structures, while, there is historically more clinical experience with fluorescein angiography interpretation. Fluorescein dye more rapidly spreads, limiting its value in cases of occult neovascularization, scarring, retinal pigment epithelial detachments, and polypoidal choroidal vasculopathy. In these types of cases, combined ICG/OCT imaging offers distinct advantages.

Finally, we have demonstrated how the signal from the SLO channel can be used to reduce movement artifacts in simultaneously captured corresponding C-scan or B-scan images. This is another unique feature of multichannel *en-Face*-OCT imaging available only in Time Domain.

### **Acknowledgments**

R. Rosen and G. Dobre acknowledge support from the Leon Lane-sponsored ARIBA Fund of the Department of Ophthalmology, New York Eye and Ear Infirmary and Ophthalmic Technologies Inc., Toronto, Canada. A. Podoleanu is grateful for the support of Ophthalmic Technologies Inc., Toronto, Canada and Superlum Moscow, Russia.